J Mater Sci (2011) 46:4384–4391
DOI 10.1007/s10853-011-5370-6

IIB 2010

Sequential HAADF-STEM observation of structural changes in Au nanoparticles supported on CeO_2

Tomoki Akita · Shingo Tanaka · Koji Tanaka · Masatake Haruta · Masanori Kohyama

Received: 27 August 2010 / Accepted: 3 February 2011 / Published online: 15 February 2011

Abstract Sequential high-angle annular dark-field scanning transmission electron microscopy (HAADF-STEM) was used to clarify the detailed process of structural changes in Au/CeO_2 catalysts found in our previous TEM observations. The layer-by-layer shrinkage of a Au nanoparticle on CeO_2 during electron beam irradiation and recovery at the same position after switching off the beam were observed with clear resolution of Ce and Au atomic columns. Displaced Au atomic columns at the perimeter of the Au/CeO_2 interface during the electron beam irradiation have been analyzed using first-principles calculations, which indicate that such Au atoms at the perimeter edge are located above oxygen vacancies or Ce-terminated surface regions. The present behavior of Au atoms and nanoparticles provides valuable insights into the mechanisms of both structural changes and catalytic activity of Au/CeO_2 catalysts.

Introduction

The catalytic performance of Au nanoparticles supported on metal oxides has been widely investigated for various reactions, including selective low-temperature CO oxidation [1], water gas shift reaction [2, 3], and liquid phase oxidation of alcohols [4, 5]. It is well known that the catalytic activity and selectivity are sensitive to the size of the Au nanoparticles, the kind of metal oxide supports used, and the Au/metal-oxide junction structure [6]. Although several models proposed so far regard Au particles as active sites, several experimental studies indicate that the perimeter around Au nanoparticles that is in contact with the metal-oxide supports plays a key role in the catalytic activity [3, 6–8]. Thus, it is crucial to investigate the detailed structures of the perimeter and the interface of Au/metal-oxide systems using electron microscopy. In particular, high-angle annular dark-field scanning transmission electron microscopy (HAADF-STEM) is a valuable tool to observe local atomic structures, as has been successfully reported for various material interfaces [9, 10]. If a small electron probe and sufficient collection angle for the annular detector are used, nearly direct images of atomic columns can be obtained without requiring great effort for interpretation via image simulations [9, 11, 12].

Among various Au/oxide support catalysts, Au/CeO_2 systems are interesting because of their high catalytic activity for the low-temperature water gas shift reaction [13–15], and the atomic and electronic structures of these systems have been investigated by various techniques [16–18]. It is well known that CeO_2 can rapidly release and store oxygen in response to a reductive and oxidative atmosphere, respectively, associated with the Ce^{4+}/Ce^{3+} redox process [19]. Recently, we carried out typical TEM observations of the fine structure of Au/CeO_2 systems and found novel dynamic structural changes in Au nanoparticles on CeO_2 surfaces [20–22]. During the TEM observations, relatively small Au nanoparticles were found to shrink layer-by-layer and eventually disappear, whereas a monolayer tends to remain. After the electron beam was turned off and the sample remained in the chamber, Au

T. Akita (✉) · S. Tanaka · K. Tanaka · M. Kohyama
Research Institute for Ubiquitous Energy Devices, National Institute of Advanced Industrial Science and Technology (AIST), 1-8-31 Midorigaoka, Ikeda, Osaka 563-8577, Japan
e-mail: t-akita@aist.go.jp

M. Haruta
Department of Applied Chemistry, Graduate School of Urban Environmental Sciences, Tokyo Metropolitan University, 1-1 Minami-Osawa, Hachioji, Tokyo 192-0397, Japan

nanoparticles were found to recover at the same positions. This was found when the TEM observations were re-started. Then, the shrinkage and disappearance of the Au particles occurred again, and the recovery occurred after the beam was turned off again. The shrinkage of Au nanoparticles on CeO_2 itself was first observed by Cochrane et al. [23], whereas the cyclic disappearance and recovery were observed for the first time in our earlier study. Recently, Majimel et al. [24] have observed a similar cyclic phenomenon using conventional TEM. However, the detailed mechanism has not yet been resolved.

The present phenomenon is likely associated with the formation and annihilation of oxygen vacancies in CeO_2 for the switching on and off of the electron beam. The formation of a high density of oxygen vacancies in CeO_2 induced by the electron beam was confirmed by electron energy-loss spectroscopy (EELS) of the O *K*-edge, where an unoccupied Ce4*f*–O2*p* hybridization peak decreased remarkably during TEM observation, due to the Ce^{4+}/Ce^{3+} redox process [22]. In contrast, recovery of this EELS peak was observed after the beam was turned off, corresponding to annihilation of oxygen vacancies due to absorption of residual oxygen gas in the chamber [22]. Oxygen vacancies on CeO_2 surfaces and Au surface diffusion seem to be involved in the present phenomenon, because the behavior of Au nanoparticles is greatly affected by a hydrogen atmosphere [21]. Note that no such structural changes in Au nanoparticles have been observed on other metal oxides where such a high density of oxygen vacancies cannot be introduced. The present structural changes in Au/CeO_2 systems should be closely related to the catalytic activity, because the shape of the Au nanoparticles, the structure of the perimeter edge, and the behavior of oxygen should be involved in the catalytic reactions.

In this study, we carried out sequential HAADF-STEM observations of the Au/CeO_2 system for the first time to investigate the mechanism of the cyclic structural change according to the switching on and off of the electron beam. In our earlier work, we obtained profile-view HAADF-STEM images of Au/CeO_2 interfaces clear resolving Au and Ce atomic columns [21]. The sequential HAADF-STEM observations can directly detect the atomic process of the structural change as well as detailed behavior of Au atoms at the perimeter edge. The observed results combined with first-principles calculations were very valuable to elucidate the mechanisms of both the structural changes and catalytic activity of the Au/CeO_2 system.

Experimental and theoretical methods

A polycrystalline CeO_2 substrate was prepared as thin crystalline samples for TEM observations by mechanical polishing and ion milling. Gold nanoparticles were deposited on a CeO_2 substrate by vacuum deposition under 10^{-6} Torr by heating a Au wire in a tungsten basket heater [22]. The Au/CeO_2 sample was then heated in air at 573 K for 4 h. The Au particle size could be controlled to some extent by changing the heating temperature. The Au/CeO_2 sample was placed in the double tilt specimen holder of the TEM. The TEM and HAADF-STEM observations were carried out using a JEOL JEM-3000F transmission electron microscope (coefficient of spherical aberration, $Cs = 0.6$ mm) equipped with a digitally processed STEM imaging system. The collection angle of the annular dark-field detector was set to 65–250 mrad. The HAADF-STEM images were obtained with 8.2 s for an image of 512 × 512 pixels. The electron probe current was about 10–20 pA at 300 keV. Noise in the HAADF-STEM images was reduced using a low-pass filter with the image processing software, Gatan Digital Micrograph. By image simulations using WinHREM (HREM Research Inc), we confirmed that the HAADF-STEM image can represent correct atomic column positions of Au and Ce as maximum intensity positions without any artifact in our observation condition.

To obtain structural and energetic insights into Au-atom or Au-layer deposition on stoichiometric (O-terminated) and reduced (Ce-terminated) CeO_2 (111) surfaces, density-functional theory (DFT) calculations of $Au/CeO_2(111)$ systems were carried out. The electron–ion interactions were dealt with using the projector augmented wave (PAW) method [25, 26], and the valence wave functions were expressed by the plane-wave basis with a cut-off energy of 40 Ry. Generalized gradient approximation (GGA) [27] was used for the exchange–correlation energy functional, and the DFT + U scheme [28, 29] was used to deal properly with on-site Coulomb and exchange interactions among Ce-4*f* electrons. A value of $U = 5$ eV was selected so as to reproduce the atomic and electronic structures and cohesive energies of both the CeO_2 and Ce_2O_3 crystals obtained in previous studies [30, 31]. The original code for the PAW scheme, QMAS (Quantum Materials Simulator) [32], was used. More details of the computational scheme and results for CeO_2, Ce_2O_3, and Au/CeO_2 systems will be provided in an upcoming paper [33].

Results and discussion

HRTEM observations

In the sample of the current work, small Au particles of about 3–5-nm diameter are supported on a CeO_2 substrate with sufficiently high density. Figure 1 shows a typical

profile-view high-resolution TEM (HRTEM) image of a Au nanoparticle on a CeO_2 substrate. The CeO_2 substrate has wide and flat low-index (111) facets. A faint Fresnel fringe appears around the Au particle, due to spherical aberration, whereas a lower Cs value and a sufficient focus condition could yield good quality images of the edge of the Au particles. For the Au/CeO_2 interface, however, it is difficult to clarify interface atomic sites from the TEM image, because the appropriate focus condition is different for the Au particle and the CeO_2 substrate. For this purpose, we need to simulate the TEM image iteratively for various model structures, which is a complicated task, due to the difficulty in determining the relative position of the Au particle along the electron beam on the CeO_2 substrate. Thus, HAADF-STEM observations were performed in this study which could estimate the position of atomic columns directly [21].

Gold particles tend to be supported on the CeO_2 surface with preferential orientational relationships of (111)[1–10]Au//(111)[1–10] CeO_2 or (111)[–110]Au//(111)[1–10]CeO_2. The latter can be formed by the inversion of the Au crystal of the former. The Au particle in Fig. 1 has the latter relationship. Although the orientation relationships between a metal particle and a metal oxide substrate should be studied in controlled experimental conditions under thermal equilibrium and be statistically estimated [34, 35], the estimation was not conducted using such detailed conditions in this experiment. However, these orientational relationships are the same as in our previous observations [20–22] for samples prepared by vacuum deposition and heating in air and for those prepared by the deposition precipitation method as practical Au catalysts. Gold particles tend to be supported on the edges of atomic steps on the CeO_2 surfaces, as observed in Fig. 1. This implies that the Au nanoparticles should initially interact weakly with clean and flat CeO_2(111) surfaces and that morphological defects should act as stable deposition sites for Au nanoparticles [18].

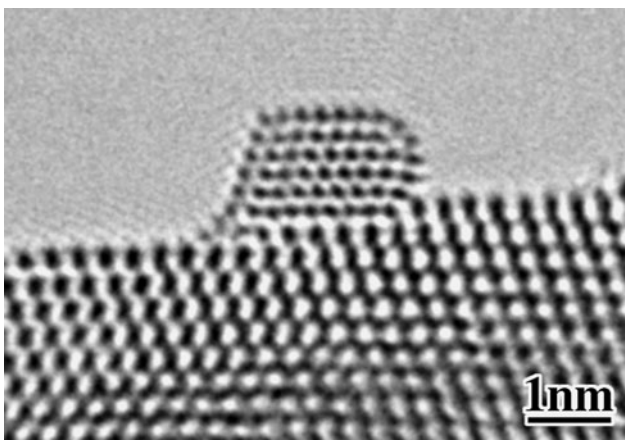

Fig. 1 Typical HRTEM image of a Au nanoparticle on CeO_2

Sequential HAADF-STEM observations

Figure 2 shows sequential HAADF-STEM images of a Au particle on CeO_2 recording the structural change as a function of time under electron beam irradiation. The HAADF-STEM images in Fig. 2a–d were obtained as snapshots during TEM and HAADF-STEM observations. The interval for recording each image was 10–30 min for the images in Fig. 2a–d. Figure 2e–h was taken sequentially within 10 min. The incident electron beam was kept parallel to the CeO_2[110] zone axis. Atomic columns of Ce and Au are observed as bright contrast, whereas oxygen columns are not detected because of the smaller atomic number. The interface has an incoherent configuration with a nearly 4:3 coincidence relation, due to the relation of fcc lattice parameters as approximately $4a_{Au} = 3a_{CeO_2}$. The Au nanoparticle is also supported on the step edge of the CeO_2(111) surface as indicated by the white arrow in Fig. 2a. The Au nanoparticle initially had a height of seven atomic layers, as seen in Fig. 2a. The lattice fringe of the Au particle appears in one direction, which means the Au particle does not have an orientation relationship of (111)[1–10]Au//(111)[1–10]CeO_2 or (111)[–110]Au//(111)[1–10]CeO_2. The crystal orientation and size of the Au nanoparticle changed during TEM and HAADF-STEM observations. In Fig. 2c, the lattice fringe of the Au particle is observed in two directions, due to the formation of the relationship (111)[–110]Au//(111)[1–10]CeO_2.

The height of the Au nanoparticle becomes smaller, from 7 (Fig. 2a) to 4 layers (Fig. 2d). The width of the Au nanoparticle becomes smaller from Fig. 2d–e, although the height of four layers is not changed. During the sequential observations shown in Fig. 2e–h, the Au nanoparticle becomes smaller layer-by-layer. The height of the Au nanoparticle changes from 4 (Fig. 2e and f) to 3 layers (Fig. 2g) to 2 layers (Fig. 2h). Surface diffusion of Au atoms from the Au nanoparticle should be activated by momentum transfer and local heating caused by electron beam irradiation, and this should be of prime importance for the shrinking of the Au nanoparticle. However, an essential point to note is that the diffused Au atoms do not seem to come back to the original Au particle or go to other Au particles, which should result in the shrinkage. This can be interpreted as occurring because of the trapping of diffusing Au atoms by a high density of oxygen vacancies on the surface or in the bulk of CeO_2. Note that no similar shrinkage was observed under similar irradiation conditions for Au nanoparticles deposited on other metal oxides where such a high density of oxygen vacancies is not generated.

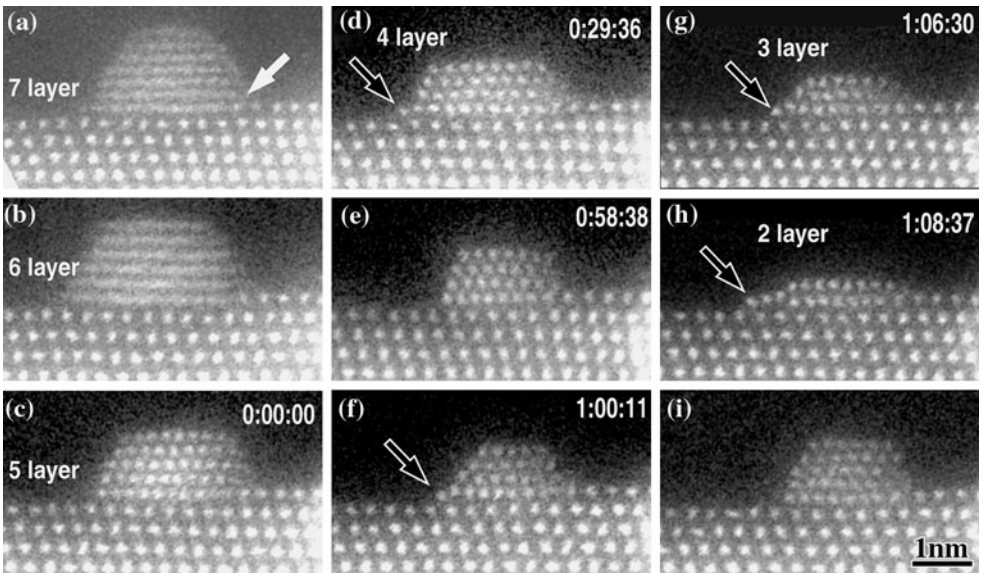

Fig. 2 Sequential HAADF-STEM images of the structural change of a Au nanoparticle on CeO_2 under electron beam irradiation. **a–d** Snapshots during TEM and HAADF-STEM observations obtained with intervals of 10–30 min, **e–h** sequential snapshots in 10-min intervals, and **i** a snapshot after 15 min without electron beam irradiation

In Fig. 2h, the Au nanoparticle has a flat raft-like shape. The area of the contact interface becomes larger than that in Fig. 2e. The Au nanoparticle with a 2-layer height has a crystalline structure with well-ordered atomic columns, although the 2-layer Au particles revealed quite different structures on a TiO_2(110) surface [36]. The flat Au nanoparticle was previously observed when the resolution was not sufficient [20, 22]. The flat shape indicates strong interfacial adhesion, and the increase in the contact area indicates enhanced interfacial adhesion during the observation. As will be discussed later, first-principles calculations show that oxygen vacancies or Ce-terminated surfaces have stronger adhesion with the Au atoms than a stoichiometric CeO_2 surface. Thus, it can be stated that the density of oxygen vacancies accumulated at the interface or surface increased gradually during the observation. This is also supported by our first-principles calculation results of lower vacancy formation energies at the CeO_2 surface and Au/CeO_2 interface compared to the bulk value [33].

After the HAADF-STEM observation shown in Fig. 2h, the sample was kept in the electron microscope without electron beam irradiation for 15 min. HAADF-STEM observation was then restarted revealing that a crystalline Au nanoparticle was recovered at the same position as in Fig. 2i. This nanoparticle with a five atomic layer height and a hemispherical shape was confirmed to be a Au particle on the basis of the crystal structure and lattice parameter. As examined in Ref. [22], the density of oxygen vacancies is greatly decreased by the absorption of residual oxygen gases in the chamber after switching off of the electron beam. Au atoms trapped at surface oxygen vacancies should be released and these diffuse again because the replacement of a trapped Au atom by oxygen is an exothermic reaction, as examined later by first-principles calculations. Au surface diffusion should be activated by thermal energy from this replacement as well as overall oxidation of a CeO_{2-x} surface.

Although the present structural changes were previously observed for samples prepared by the deposition precipitation method or by the vacuum deposition method, the present sequential HAADF-STEM observations have revealed detailed behavior of atomic columns during the process of the structural change. However, HAADF-STEM cannot observe isolated diffusing Au atoms, due to the detection limits in time and sensitivity. Thus, we cannot strictly conclude whether Au atoms diffuse on the CeO_2 surface or into the bulk CeO_2, or whether the diffused Au atoms are trapped by surface oxygen vacancies or by bulk oxygen vacancies. In any case, it is apparent that Au atoms do not vaporize, and the recovery of Au particles means that diffused Au atoms should exist near the Au particles.

Au atoms at the perimeter edge

In the present observations, we also observed for the first time the peculiar behavior of Au atomic columns at the perimeter, which should be related to the dynamical process of Au surface diffusion and structural changes. Additional Au atomic columns appear at the perimeter of the Au/CeO_2 interface as indicated by an arrow in Fig. 2d, f, g, and h. The atomic positions of these Au columns are deviated from the exact crystal positions of the Au

nanoparticle. The image of each deviated column is not caused by an isolated Au atom, but by several atoms along the beam direction, due to the image intensity is strong enough. Figure 3a and b shows HAADF-STEM images of the perimeter region of the same Au nanoparticle on CeO_2 as in Fig. 2 with a schematic drawing of the atomic column positions. The deviated Au atomic column at the perimeter edge is indicated by an arrow in Fig. 3a. The neighboring Au atomic column is also displaced in Fig. 3a and b. From 25 HAADF-STEM images observed for the same Au nanoparticle with different shapes in the shrinkage process, including Figs. 2 and 3a, the projected positions of the displaced Au columns at the perimeter edge relative to the neighboring Ce atomic columns are plotted as black dots in Fig. 3c. All of these positions are similar around the average position indicated by a gray circle. This means that the displaced Au atoms at the perimeter edge should be located on some common stable sites. The averaged position is 0.24 nm height from the top Ce atomic layer, which is slightly lower than the mean interfacial Au–Ce interlayer distance, 0.28 nm [21]. The horizontal position is 0.19 nm from the lower-left Ce column, a little right of the center between the two Ce atomic columns.

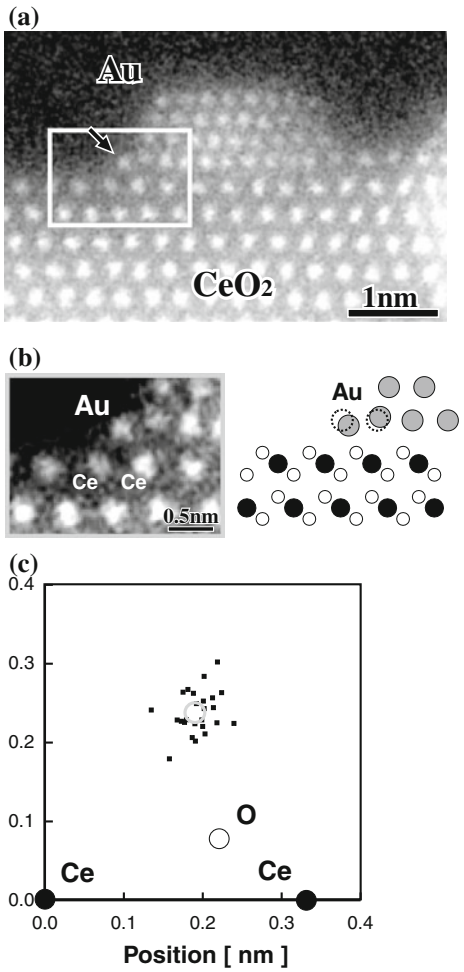

Fig. 3 HAADF-STEM image of a Au nanoparticle on CeO_2 (the same as in Fig. 2), and analysis of atomic column positions at the perimeter. **a** HAADF-STEM image, **b** enlarged image at the perimeter and a corresponding structure model, and **c** projected positions of the Au atomic column at the perimeter as obtained from 25 observed HAADF-STEM images, relative to the positions of neighboring Ce atomic columns, with the average position indicated by a gray circle

Figure 4 shows schematic structure models of Au atomic columns on stoichiometric (O-terminated) and reduced (Ce-terminated) $CeO_2(111)$ surfaces in profile and plan views. The stoichiometric $CeO_2(111)$ surface is known to be stable under atmospheric pressure, and even in an ultra-high vacuum ($<10^{-6}$ Pa) [37, 38]. In profile views from the [-110] direction in Fig. 4, one Au column is located at the averaged position of the displaced Au columns at the perimeter edge. This averaged position can be regarded as deposition on a 3-fold hollow site (H3 site, explained in detail later) for the Ce-terminated $CeO_2(111)$ surface and as deposition on an on-top site or a bridge site of oxygen atoms for the O-terminated $CeO_2(111)$ surface. Not all Au atoms in this column are located on identical sites, due to the incoherent arrangement of Au atoms along the column. The 3-fold hollow site of the Ce-terminated $CeO_2(111)$ surface is the same as the oxygen-vacancy site of the O-terminated surface.

From the averaged height of the Au atoms at the perimeter edge, which is lower than the interfacial Au–Ce distance, such Au atoms are assumed to be located above oxygen vacancies or on a Ce-terminated surface region. Oxygen vacancies are formed in bulk CeO_2 by electron beam irradiation as confirmed by EELS analysis [22]. Oxygen vacancies and their clusters are more readily created on the CeO_2 surface [38], and vacancies created in the bulk should diffuse to the surface or interface, due to the lower oxygen-vacancy formation energy at the surface or interface [33].

First-principles calculations

To examine the above argument, first-principles calculations were carried out for Au-monolayer deposition on O-terminated (stoichiometric) and Ce-terminated (reduced) $CeO_2(111)$ surfaces. We deal with (1×1) coherent deposition models for a $CeO_2(111)$ slab, consisting of five sets of O–Ce–O layers for the O-terminated case. For both termination cases, three kinds of symmetric adsorption sites, T1, T4, and H3, were examined, which are respectively the on-top site, the 3-fold site just above the second-layer atom, and the 3-fold hollow site. The stable Au–Ce interlayer distances obtained for the T1, T4, and H3 adsorptions on the O-terminated surface are 0.31, 0.32, and 0.28 nm, respectively, and those on the Ce-terminated

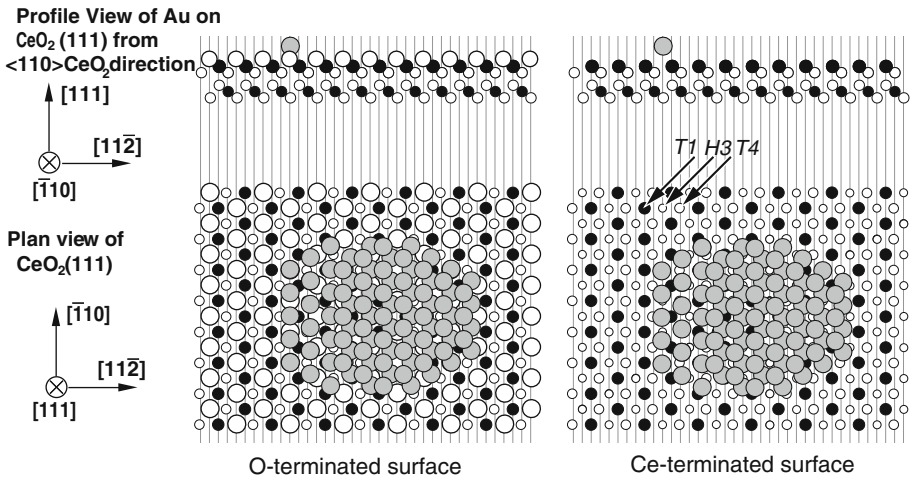

Fig. 4 Schematic drawings of structural models of Au atomic columns on O-terminated (stoichiometric) and Ce-terminated (reduced) $CeO_2(111)$ surfaces. *Smaller closed* and *open circles* indicate Ce and O atoms, respectively, and *larger gray* and *open circles* indicate Au atoms and top-layer O atoms, respectively. The T1, T4, and H3 sites are explained in the text

surface are 0.28, 0.22, and 0.21 nm. We also examined a Au atom trapped at a surface oxygen vacancy by the (3 × 3) cell, where the distance between the Au atom and the top Ce layer is similar to that for H3 adsorption on the Ce-terminated surface. By taking into consideration the probable incoherent arrangement of Au atoms along the column due to the 4:3 relation, the calculated results indicate that the Au–Ce interlayer distance should be around 0.3 nm, and cannot be less than 0.28 nm, for the O-terminated case, whereas it can be less than 0.3 nm for the Ce-terminated case or for the O-terminated case with rich oxygen vacancies. Thus, Au atoms of the displaced atomic column at the perimeter edge can be said to be located above oxygen vacancies or a Ce-terminated surface region.

In the present calculations, the most stable site for the O-terminated case is T1 with adhesion energy of 0.11 eV per Au atom, whereas that for the Ce-terminated case is H3 with adhesion energy of 3.2 eV. Larger adhesion energy for the Ce-terminated interface does not necessarily mean stability of the Ce-terminated interface compared to the O-terminated interface, because the relative stability depends on the free energy as a function of chemical potentials. However, the relative stability of the Ce-terminated one should be enhanced under the oxygen-deficient condition by the electron beam irradiation [33]. Since the Ce-terminated surface reveals stronger adhesion with Au atoms, the trapping energy for Au atom by a surface oxygen vacancy should be sufficiently strong to affect Au surface diffusion. The calculated trapping energy of the surface oxygen vacancy in the (3 × 3) cell is 2.18 eV against a free Au atom, and 1.52 eV against a Au atom on the O-terminated $CeO_2(111)$ surface. The flat shape of the Au nanoparticle and the extension of the interfacial area observed in Fig. 2h is likely caused by stronger Au-substrate adhesion due to accumulation of oxygen vacancies at the CeO_2 surface or interface during the electron beam irradiation. The behavior of displaced Au columns at the perimeter edge should be caused by a similar origin.

As discussed above, the recovery of Au nanoparticles is considered to occur via the release of Au atoms trapped at oxygen vacancies, due to the absorption of residual oxygen in the chamber. The energy gain in the replacement of a trapped Au atom by oxygen at the surface vacancy is 1.12 eV from our first-principles results. This gain should activate Au surface diffusion as well as thermal energies by the recovery of a surface oxygen vacancy and a bulk oxygen vacancy, with values of 2.64 and 3.61 eV, respectively, as our first-principles results of the formation energies [33].

All the present observations combined with first-principles results support the following model of the cyclic structural change. Diffusing Au atoms from Au nanoparticles activated by the electron beam are trapped by surface oxygen vacancies of CeO_2 induced by the electron beam. This causes shrinkage of the Au nanoparticles, while one or two layers remain because of the stronger Au-substrate adhesion by accumulation of oxygen vacancies at the interface. After the beam is turned off, the trapped Au atoms are released by the absorption of residual oxygen exothermically, activating Au surface diffusion again and resulting in rapid recovery of Au nanoparticles. Note, experimentally, diffusing and trapped Au atoms have not yet been detected directly. This will be the subject of a future study.

Discussion

About the averaged position of the displaced Au atomic column at the perimeter edge in Fig. 3c, here we discuss the accuracy of the data. Each black dot in Fig. 3c was obtained as a maximum intensity point at the displaced atomic column in each HAADF-STEM image in the

sequential observation of the shrinkage process of a common Au particle on a CeO_2 surface. It should be noted that the identification of the column position via the maximum intensity point itself is quite natural in the HAADF-STEM scheme, due to rare occurrence of artifacts in usual conditions as examined in the image simulations mentioned above (See the section of Experimental and theoretical methods). This is quite different from usual HRTEM images where intensive image simulations are essential to decide atomic positions due to significant occurrence of artifacts, especially at surfaces or interfaces. Of course, for the Au atomic column at the perimeter edge, relatively short column lengths along the electron beam and random displacements of each atom by thermal effects or incoherency with the CeO_2 surface result in weak or broadened images of the atomic column, leading to some errors in determining the column position. This is in contrast to the Ce column positions with high accuracy by clear column images due to thick column lengths and common stable substrate structure. However, our purpose is to decide the averaged position of the edge atomic column, or the averaged position of atoms in the edge atomic column, as indicated by the gray circle in Fig. 3c. We would like to say that the final averaged position or the final conclusion of our argument using the averaged position is not changed, even if we consider the error problem of each plot point. The average was obtained by more data, and each maximum intensity point is some kind of average of atomic positions in each column. In other words, we can regard the dispersion of the black dots in Fig. 3c as the extent of practical errors (standard deviation: 0.03 nm) to decide the averaged position.

About the possibility of containing Ce atoms in the displaced atomic column at the perimeter, we can deny the presence of pure Ce columns or a large percentage of Ce atoms in such columns by considering the results of first-principles calculations of a Ce-terminated CeO_2(111) surface. The Ce-terminated CeO_2 surface cannot be stabilized even in the present reductive atmosphere under electron beam irradiation, except for the case of Au-layer deposition, in the analysis of free energies depending on oxygen chemical potentials [33]. And even in the Au/CeO_2 systems, interface Ce atoms have back bonds with oxygen atoms. Thus, we cannot say that bare Ce atomic columns on the CeO_2 surface can be stabilized in the present experimental condition. In addition, if a high concentration of Ce atoms were contained, the mobile behavior of the edge atomic column after turning off the electron beam should be seriously affected, due to the formation of CeO_2 at the perimeter edge via remaining oxygen gasses in the chamber. However, the edge column rapidly disappears as shown in Fig. 2i after switching off the beam, which indicates no inclusion of a high concentration of Ce atoms. Of course, we cannot completely deny the possibility that a small amount of Ce atoms might be contained in the Au atomic column at the perimeter edge. However, this point has no substantial effects on our argument of the mechanism of the structural change of Au particles on CeO_2 in this study.

About the possibility of containing Ce atoms at the interface Au layer, the inclusion of Ce atoms into deposited Au particles was observed in the experiments using a much stronger electron beam with a dose over ten times higher than the usual one [22]. In such observations, under more reductive atmosphere, reduced Ce atoms seem to be contained into Au particles, and CeO_x layers covering each Au particle are formed after switching off the beam. This encapsulation prevents usual cyclic shrinkage and recovery. However, in the present experimental condition to observe usual cyclic shrinkage and recovery of Au particles, we can deny the possibility that a high concentration of Ce atoms are contained in the interface Au layer, from the features of the HAADF-STEM images. As shown in Fig. 2, basically the interface Au layers reveal local configurations like fcc Au even in the two-layer structure, while the columns at the perimeter edge show some displacements. This indicates that the interface layer mainly consists of Au. We do not observe the encapsulation in the present observation condition. Of course, we cannot deny the possibility that a small amount of Ce atoms might be contained in the interface Au layer, just as the above argument on the perimeter column. To examine this problem in detail is beyond the present study, while this problem has no serious effects on our present conclusion.

Finally, although reduction of the CeO_2 substrates occurs under electron beam irradiation in the present experiments, and the atmosphere is quite different from that of real catalytic reactions, we would like to emphasize that the structure of the perimeter of the Au particles in an oxygen-deficient condition is important to understand the catalytic activity of Au/CeO_2 catalysts. A proposed mechanism of CO oxidation includes the process of reduction of metal oxide support [7]. The water gas shift reaction occurs in a hydrogen-rich reductive atmosphere, and the proposed reaction mechanism also includes the removal of oxygen at the perimeter region [15].

Conclusions

Cyclic structural changes of Au nanoparticles deposited on CeO_2 by the switching on and off of an electron beam were investigated by sequential HAADF-STEM observations, which clarified the detailed process of layer-by-layer shrinkage and recovery of a Au nanoparticle. Atomic-structure change at the perimeter of the Au/CeO_2 interface

was observed for the first time owing to the atomic resolution of the HAADF-STEM instrument used in this study. Comparison with DFT first-principles calculations indicates that displaced Au atoms at the perimeter edge are bonded to oxygen vacancies or Ce-terminated surface regions. The present results support a mechanism dominated by the behavior of oxygen vacancies and diffusing Au atoms. The present results are also valuable to investigate the mechanism of catalytic activity of Au/CeO_2 catalysts. The perimeter is considered to be catalytic active sites for oxidation reactions, and oxygen atoms on the CeO_2 surface near the perimeter are considered to contribute to the catalytic reactions.

Acknowledgement This study was supported by the Japan Society for the Promotion of Science (JSPS-Grant-in-Aid for Scientific Research (B) (18360322) and Grant-in-Aid for Specially Promoted Research (19001005)). The authors are grateful to Ms. J. Maekawa for her assistance with sample preparation.

References

1. Haruta M, Kobayashi T, Sano H, Yamada N (1987) Chem Lett 405
2. Andreeva D (2002) Gold Bull 356:82
3. Tibiletti D, Amieiro-Fonseca A, Burch R, Chen Y, Fisher JM, Goguet A, Hardacre C, Hu P, Thompsett D (2005) J Phys Chem B 109:22553
4. Prati L, Rossi M (1998) J Catal 176:552
5. Abad A, Concepción P, Corma A, García H (2005) Angew Chem Int Ed 44:4066
6. Haruta M (2003) Chem Rec 3:75
7. Bond GC, Thompson DT (2000) Gold Bull 33:41
8. Fujitani T, Nakamura I, Akita T, Okumura M, Haruta M (2009) Angew Chem Int Ed 48:9515
9. Browning ND, Pennycook SJ (1996) J Phys D Appl Phys 29:1779
10. Buban JP, Matsunaga K, Chen J, Shibata N, Ching WY, Yamamoto T, Ikuhara Y (2006) Science 311:212
11. Pennycook SJ, Boatner LA (1988) Nature 336:565
12. Pennycook SJ, Jesson DE (1991) Ultramicroscopy 37:14
13. Fu Q, Weber A, Flytzani-Stephanopoulos M (2001) Catal Lett 77:87
14. Sakurai H, Akita T, Tsubota S, Kiuchi M, Haruta M (2005) Appl Catal A Gen 291:179
15. Burch R (2006) Phys Chem Chem Phys 8:5483
16. Fu Q, Flytzani-Stephanopoulos M (2003) Science 301:935
17. Manzoli M, Boccuzzi B, Chiorino A, Vindigni F, Deng W, Flytzani-stephanopoulos M (2007) J Catal 245:308
18. Lu JL, Gao HJ, Shaikhutdinov S, Freund HJ (2007) Catal Lett 114:8
19. Trovarelli A (2002) Catalysis by ceria and related materials. Imperial College Press, London
20. Akita T, Okumura M, Tanaka K, Kohyama M, Haruta M (2005) J Mater Sci 40:3101. doi:10.1007/s10853-005-2670-8
21. Akita T, Tanaka K, Kohyama M (2008) J Mater Sci 43:3917. doi:10.1007/s10853-007-2401-4
22. Akita T, Okumura M, Tanaka K, Kohyama M, Haruta M (2006) Catal Today 117:62
23. Cochrane HD, Hutchison JL, White D, Parkinson GM, Dupas C, Scott AJ (1990) Ultramicroscopy 34:10
24. Majimel J, Lamirand-Majimel M, Moog I, Feral-Martin C, Tre′guer-Delapierre M (2009) J Phys Chem C 113:9275
25. Blöchl PE (1994) Phys Rev B 50:17953
26. Kresse G, Joubert D (1999) Phys Rev B 59:1758
27. Perdew JP, Burke K, Ernzerhof M (1996) Phys Rev Lett 77:3865
28. Anisimov VI, Solovyev IV, Korotin MA, Czyzyk MT, Sawatzky GA (1993) Phys Rev B 48:16929
29. Dudarev SL, Botton G, Savrasov SY, Humphreys CJ, Sutton AP (1998) Phys Rev B 57:1505
30. Nolan M, Fearon JE, Watson GW (2006) Solid State Ion 177:3069
31. Andersson DA, Simak SI, Johansson B, Abrikosov IA, Skorodumova NV (2007) Phys Rev B 75:035109
32. Ishibashi S, Tamura T, Tanaka S, Kohyama M, Terakura K (2007) Phys Rev B 76:153310
33. Tanaka S, Akita T, Kohyama M, Takeda S, (in preparation)
34. Sadan H, Kaplan WD (2006) J Mater Sci 41:5099. doi:10.1007/s10853-006-0437-5
35. Sadan H, Kaplan WD (2006) J Mater Sci 41:5371. doi:10.1007/s10853-006-0407-y
36. Shibata N, Goto A, Matsunaga K, Mizoguchi T, Findlay SD, Yamamoto T, Ikuhara Y (2009) Phys Rev Lett 102:136105
37. Esch F, Fabris S, Zhou L, Montini T, Africh C, Fomasiero P, Comelli G, Rosei R (2005) Science 309:752
38. Namai Y, Fukui K, Iwasawa Y (2003) J Phys Chem B 107:11666